Rock Mech Rock Eng (2015) 48:143–157
DOI 10.1007/s00603-014-0550-8

ORIGINAL PAPER

Evaluation of Mode I Fracture Toughness Assisted by the Numerical Determination of *K*-Resistance

Takahiro Funatsu · Norikazu Shimizu · Mahinda Kuruppu · Kikuo Matsui

Received: 18 February 2013 / Accepted: 26 January 2014 / Published online: 17 February 2014

Abstract The fracture toughness of a rock often varies depending on the specimen shape and the loading type used to measure it. To investigate the mode I fracture toughness using semi-circular bend (SCB) specimens, we experimentally studied the fracture toughness using SCB and chevron bend (CB) specimens, the latter being one of the specimens used extensively as an International Society for Rock Mechanics (ISRM) suggested method, for comparison. The mode I fracture toughness measured using SCB specimens is lower than both the level I and level II fracture toughness values measured using CB specimens. A numerical study based on discontinuum mechanics was conducted using a two-dimensional distinct element method (DEM) for evaluating crack propagation in the SCB specimen during loading. The numerical results indicate subcritical crack growth as well as sudden crack propagation when the load reaches the maximum. A *K*-resistance curve is drawn using the crack extension and the load at the point of evaluation. The fracture toughness evaluated by the *K*-resistance curve is in agreement with the level II fracture toughness measured using CB specimens. Therefore, the SCB specimen yields an improved value for fracture toughness when the increase of *K*-resistance with stable crack propagation is considered.

Keywords Fracture toughness · SCB specimen · Fracture process zone · DEM · *K*-resistance curve

List of Symbols

a	Notch length
a_0	Chevron tip distance from the specimen surface
A_3	Coefficient of the higher-order non-singular term in the crack tip stress function
$A_{\min}$	Minimum normalized stress intensity factor for the CB specimen
BDT	Uncracked Brazilian disk test
CB	Chevron bend
CCNBD	Cracked chevron-notched Brazilian disk
COD	Crack-opening displacement
CSTBD	Cracked straight-through Brazilian disk
D	Diameter of specimen
DEM	Distinct element method
E_{50}	Tangent Young's modulus at half the compressive strength
F	Load
F_c	Load at the evaluation point for the CB specimen
$F_{\max}$	Maximum load
FEM	Finite element method
FPZ	Fracture process zone
K_{Ic}	Mode I fracture toughness
K_{CB}	Level I fracture toughness measured using the CB specimen

T. Funatsu (✉)
National Institute of Advanced Industrial Science and Technology (AIST), Central 7, 1-1-1 Higashi, Tsukuba, Ibaraki 305-8567, Japan
e-mail: funatsu-t@aist.go.jp

N. Shimizu
Yamaguchi University, 2-16-1 Tokiwadai, Ube, Yamaguchi 755-8611, Japan

M. Kuruppu
Curtin University, Locked Bag 30, Kalgoorlie, WA 6433, Australia

K. Matsui
Kyushu University, 744 Motooka, Nishi-ku, Fukuoka 819-0395, Japan

K_{CB}^{c}	Level II fracture toughness measured using the CB specimen
K_{SR}	Level I fracture toughness measured using the SR specimen
K_{SR}^{c}	Level II fracture toughness measured using the SR specimen
LEFM	Linear elastic fracture mechanics
LPD	Load-point displacement
MTS	Maximum tangential stress
p	Degree of nonlinearity
R	SCB specimen radius
r_c	Radius of the FPZ
t	SCB specimen thickness
S	Half span length of support rollers
SCB	Semi-circular bend
SECRBB	Single edge cracked round bar bend
SNDB	Straight notched disk bending
SR	Short rod
UCS	Uniaxial compressive strength
XRD	X-ray diffractometry
Y	Normalized stress intensity factor
σ_c	Uniaxial compressive strength
σ_t	Tensile strength
Δa	Crack extension
β	Ratio of notch length to specimen radius
v	Poisson's ratio

1 Introduction

In rock engineering problems dealing with the stability of structures, controlling crack initiation and propagation is very important. Microcracks and macrocracks affect the rock mass strength and deformation; these factors strongly influence the stability of geological structures such as underground and open pit mines, tunnels, and rock slopes. Rock fracturing also plays a key role in the exploitation of energy resources in that creating new cracks enhances the production of oil, natural gas, and geothermal energy, and also facilitates leakage paths in the sequestration of CO_2 in geological storage sites.

The fracture toughness is a measure of a material's resistance to crack propagation. The fracture toughness of rock materials has been determined using various test specimen configurations and methods. The International Society for Rock Mechanics (ISRM) has incorporated chevron bend (CB) (ISRM 1988), short rod (SR) (ISRM 1988), and cracked chevron-notched Brazilian disk (CCNBD) (Fowell 1995) specimens into the standard method for the measurement of the fracture toughness of rock materials. Three-point bending-type specimens such as single edge cracked round bar bend (SECRBB) (Ouchterlony 1981), semi-circular bend (SCB) (Chong and Kuruppu 1988), and straight notched disk bending (SNDB) (Tutluoglu and Keles 2011) specimens, as well as Brazilian disk-type specimens such as cracked straight-through Brazilian disk (CSTBD) (Fowell and Xu 1994) and flattened Brazilian disk (Wang and Xing 1999) specimens, have also been used for the measurement of the fracture toughness. Among these, the fracture toughness measurement method using the SCB specimen shown in Fig. 1 has been recently approved as an ISRM suggested method (Kuruppu et al. 2014). It is a core-based specimen that possesses inherently favorable characteristics such as simplicity, minimal machining requirements, and easy testability through the application of three-point compressive loading using a standard test frame.

It is observed that, for the same rock sample, the mode I fracture toughness varies when different specimen types are used for measurement. Chang et al. (2002) measured the fracture toughness of granite and marble using CB, CCNBD, SCB, chevron-notched SCB, and uncracked Brazilian disk test (BDT) (Guo et al. 1993) specimens. The mode I fracture toughness values of granite and marble measured using SCB specimens were 0.68 ± 0.19 MPam$^{0.5}$ with 31 specimens and 0.87 ± 0.15 MPam$^{0.5}$ with 27 specimens, respectively. These values are lower than the fracture toughness values measured using other specimens. Khan and Al-Shayea (2000) measured the fracture toughness of limestone using SCB, CSTBD, CCNBD, and SECRBB specimens; the average values measured using the SCB, CSTBD, CCNBD, and SECRBB specimens were 0.68, 0.42, 0.61, and 0.55 MPam$^{0.5}$, respectively. Tutluoglu and Keles (2011) found that the fracture toughness values of andesite measured using CCNBD, SCB, and SNDB specimens were 1.45 ± 0.06 MPam$^{0.5}$ with five specimens, 0.94 ± 0.12 MPam$^{0.5}$ with 21 specimens, and 1.00 ± 0.09 MPam$^{0.5}$ with 20 specimens, respectively. They argued that the variation of the fracture toughness was due to the differences in the size of the fracture process zone (FPZ). They evaluated the size of the FPZ of SCB and SNDB specimens and found that the size of the FPZ of the former was 2.15 times larger than that of the FPZ of the latter. Aliha et al. (2012) reported that the fracture toughness strongly depends on the geometry and loading conditions of the test specimen. They showed that the fracture toughness of Guiting limestone measured using an SCB specimen was higher than that measured using a CSTBD specimen, and they discussed the difference between the values using the maximum tangential stress (MTS) criterion. They found that the higher-order stress term A_3 was responsible for the variation of the fracture toughness. Iqbal and Mohanty (2007) showed that the fracture toughness values of CB and CCNBD specimens for a brittle rock were comparable.

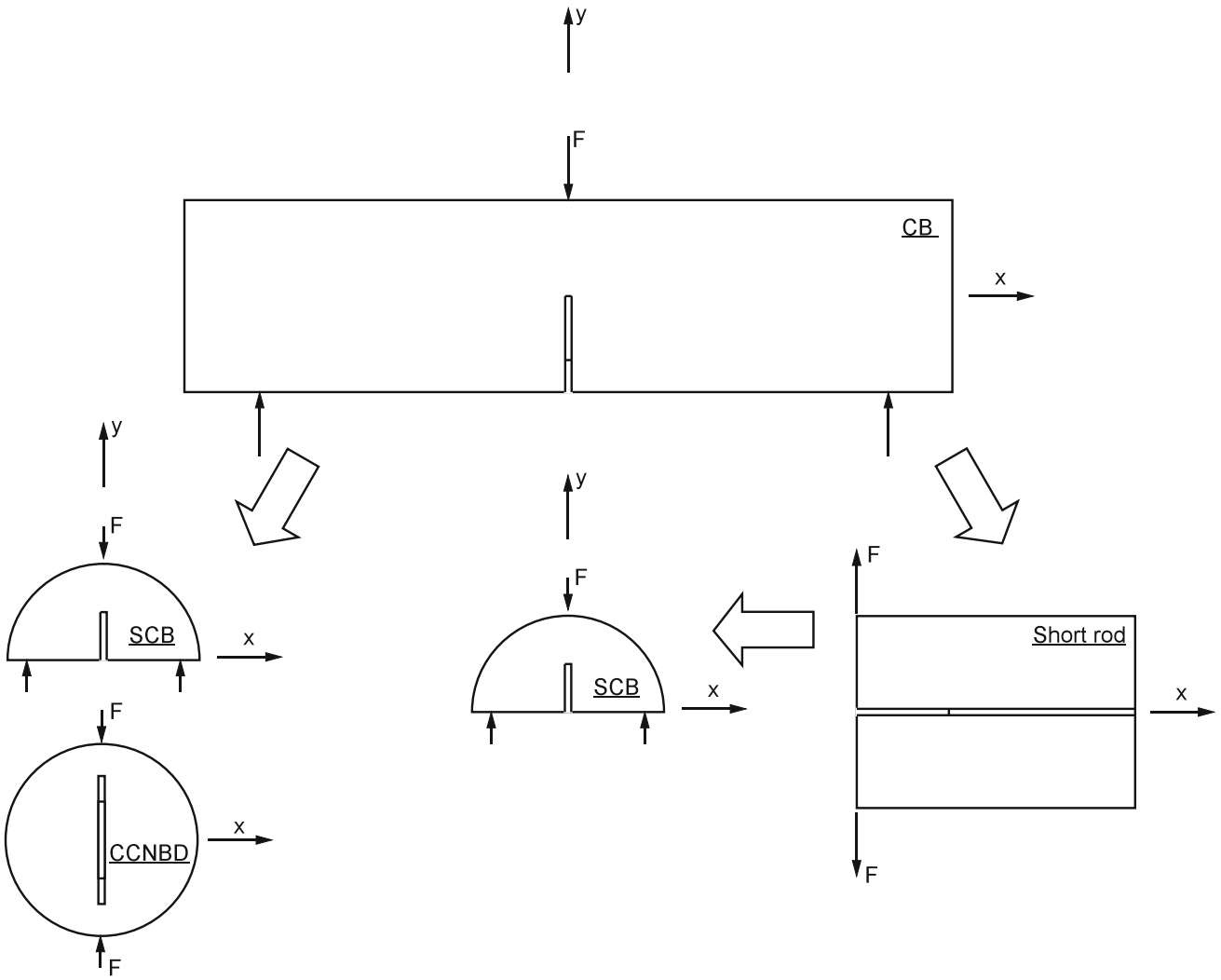

Fig. 1 Core-based fracture toughness test specimens illustrating their application to anisotropic materials [modified from Chong and Kuruppu (1988)]

These studies indicate that the fracture toughness must be dealt with carefully if it is considered representative of the rock material, especially if a non-ISRM suggested method is adopted. The size of the FPZ and pre-critical stable crack growth are the key factors affecting the fracture toughness. Nasseri et al. (2006) measured the fracture toughness and acoustic emission activity in brittle rocks. They found that the variation of fracture toughness is caused by the pre-existing microcrack density and its orientation with respect to the fracture propagation direction. The creation of an FPZ surrounding the propagating main crack has been confirmed by acoustic emission techniques. Dai et al. (2007) investigated the effect of crack–microcrack interaction on the anisotropic behavior of fracture toughness. The microstructural investigation of thin sections indicated that the pre-existing microcracks caused the variation of the fracture toughness values. The FPZ or crack growth can be estimated in several ways. Optical methods are used to observe moiré fringe patterns during loading and to measure the size of the FPZ. Acoustic emission measurement is also used to estimate the size of the FPZ. The compliance is used to indirectly measure the crack growth during loading. Apart from laboratory studies, numerical modeling is also useful for estimating the crack growth. We investigated the application of the distinct element method (DEM) (Cundall and Strack 1979), which is based on discontinuum mechanics, because crack propagation and microcracking occur in a discontinuous manner. DEM has been used to study crack propagation in rocks or rock-like materials such as concrete. For example, Azevedo and Lemos (2006) presented a DEM/finite element method (FEM) coupling algorithm which enables DEM to be used in the discretization of the fracture zone and for the surrounding areas of a discretization based on

Table 1 Mechanical properties of Kimachi sandstone

σ_c (MPa)	E_{50} (GPa)	ν	σ_t (MPa)
66.9	13.2	0.18	4.9

the FEM. The hybrid DEM/FEM method was applied for fracture analysis in concrete. They successfully modeled the crack localization process and pre-peak load versus displacement curves of both mode I and mixed mode fracture experiments performed using beam specimens. Tan et al. (2009) used the DEM software package PFC2D (Itasca Consulting Group Inc. 2004) for modeling the fracture and damage processes of polycrystalline silicon carbide (SiC) ceramics. They modeled the fracture toughness testing using a specimen subjected to three-point bend loading and showed that the numerical results agreed with the experimental measurements. D'Addetta et al. (2002) presented a combined particle and lattice model as an improved DEM formulation. It was applied to model the fracture process of cohesive granular materials somewhat similar to sandstone. They were successful in showing the typical microcrack nucleation, growth, and coalescence to form macrocracks under tension, compression, and shear modes of loading. Their simulation results were in agreement with the experimental observations. These studies demonstrate that DEM can be used for simulating the mechanical behavior of rocks and crack propagation behavior, and that it is a useful tool for investigating the FPZ and crack growth during loading.

In this study, we investigated the mode I fracture toughness using an SCB specimen. Furthermore, we used a CB specimen for the purpose of comparison of the fracture toughness. A DEM model of the SCB test specimen was used to investigate the crack growth and FPZ during loading. We evaluated the mode I fracture toughness using the SCB specimen and its *K*-resistance curve and found that the corrected mode I fracture toughness is comparable to the level II fracture toughness measured using the CB specimen.

2 Methodology

2.1 Test Material

Kimachi sandstone produced in Shimane Prefecture, Japan, was used as the test material. The mechanical properties of the rock are listed in Table 1. An analysis of this material using X-ray diffractometry (XRD) revealed that it mainly consists of albite, anorthite, quartz, montmorillonite, and mordenite.

Kimachi sandstone has been found to be slightly anisotropic (Funatsu et al. 2004). The principal directions of anisotropy are known as arrester, divider, and short-transverse. All tests using SCB and CB specimens reported herein were performed in the arrester orientation.

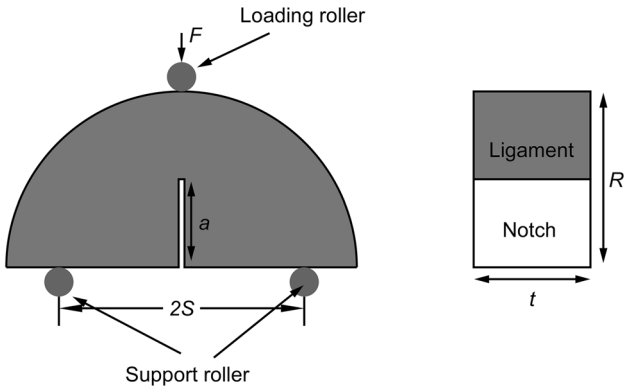

Fig. 2 Semi-circular bend (SCB) specimen geometry and schematic loading arrangement (*R* radius of the specimen, *t* thickness, *a* notch length, 2*S* distance between the two supporting pins, *F* monotonically increasing compressive load applied at the central loading pin of the three-point bend loading)

2.2 Experimental Method

2.2.1 Testing

The tests were carried out using the SCB specimen configuration shown in Fig. 1. Such an SCB specimen can be made from leftover core material after testing CB or SR specimens, so that the variation of the material properties of the rock is kept to a minimum. This specimen has certain inherently favorable properties such as simplicity, minimal machining requirements, and easy testability by means of three-point compressive loading using a standard test frame (Fig. 2).

Specimens were prepared by sawing or slicing rock cores that were drilled in the direction of bedding planes. Each resulting disk was then cut into two halves, along a plane parallel to the direction of the bedding planes, to form two specimens. Specimens of 50-mm radius and 25-mm thickness were used. A straight notch was introduced in each specimen using a diamond circular saw, such that the notch-length-to-radius ratio was 0.3, 0.4, or 0.5. The thickness of the saw blade used was 0.3 mm, yielding a notch of similar thickness. The resulting SCB test specimens had their notches in the arrester orientation with respect to the material anisotropy (Chong et al. 1987). The specimens were oven-dried at 40 °C for 120 h, and all dimensions were recorded.

The specimens were placed on the loading platform such that the span ratio *S*/*R* was 0.8 and then tested to failure under load-line displacement control and at a loading rate of 0.075 mm/min (see Fig. 3). The load, load-point displacement (LPD), and crack-opening displacement (COD) were recorded as functions of time during each test.

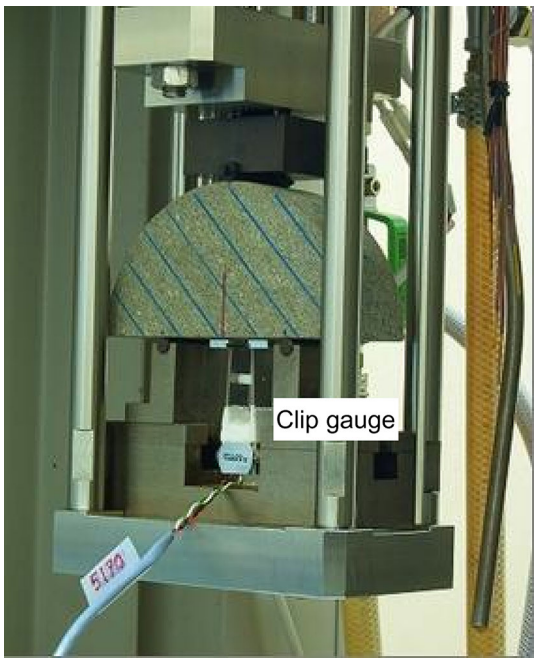

Fig. 3 Sample setup in the loading frame with a crack-opening displacement (COD) gauge

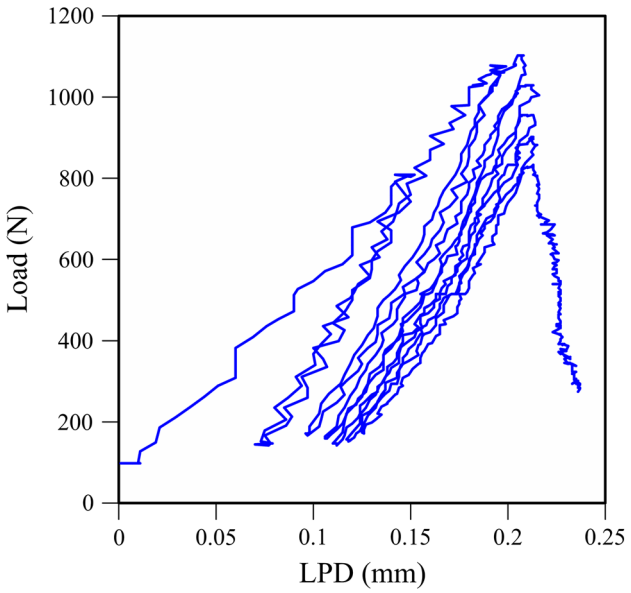

Fig. 4 Load versus load-point displacement (LPD) curve obtained by the chevron bend (CB) test also showing partial unloading cycles to facilitate determining the level II fracture toughness

2.2.2 *Derivation of Fracture Toughness by the SCB Specimen*

The fracture toughness, K_{Ic}, is determined using the peak load, non-dimensional stress intensity factor, and specimen dimensions. For the SCB specimens, K_{SCB} is given as (Chong et al. 1987):

$$K_{SCB} = Y\sigma_0\sqrt{\pi a} \tag{1}$$

where Y is the normalized stress intensity factor, $\sigma_0 = F_{max}/2Rt$, F_{max} is the maximum load, a is the notch length, R is the specimen radius, and t is the thickness. The stress intensity factor Y is a function of the a/R ratio, β, and the half-span-to-radius ratio S/R. The best-fit curve for Y is given by Lim et al. (1994) as:

$$Y = \frac{S}{R}\left(2.91 + 54.39\beta - 391.4\beta^2 + 1210.6\beta^3 - 1650\beta^4 + 875.9\beta^5\right) \tag{2}$$

where S is the half-span length of the support rollers. Equation (2) is valid for $0.1 \leq \beta \leq 0.8$. An S/R ratio of 0.8 was chosen for the fracture toughness tests performed with the SCB specimen.

2.2.3 *CB Specimen*

Fracture toughness measurement by a CB specimen is one of the ISRM suggested methods. The evaluation of fracture toughness is done at two levels. The level I fracture toughness based on fracture load is suitable if the testing material is considered as a linear elastic material. The curve of the normalized stress intensity factor versus notch length for a chevron notch has a minimum value, suggesting that the initial crack growth occurs stably and that the specimen fails upon reaching the minimum value of the stress intensity factor corresponding to the maximum applied load. Therefore, the minimum normalized stress intensity factor is used for evaluating the level I fracture toughness. For nonlinearly behaving materials, the level II fracture toughness corrects the level I fracture toughness by considering the degree of nonlinearity p. Figure 4 shows a typical load versus LPD curve.

The level I fracture toughness, K_{CB}, can be calculated by the following equation (ISRM 1988):

$$K_{CB} = A_{min}F_{max}/D^{1.5} \tag{3}$$

where F_{max} is the maximum load, D is the diameter of the specimen, and:

$$A_{min} = \left[1.835 + 7.15a_0/D + 9.85(a_0/D)^2\right]2S/D \tag{4}$$

where S is the half-span length between support points and a_0 is the chevron tip distance from the specimen surface.

The level II fracture toughness can be calculated as:

$$K_{CB}^{c} = \sqrt{(1+p)/(1-p)}F_c/F_{max}K_{CB} \tag{5}$$

where p is the degree of nonlinearity and F_c is the load at the evaluation point. Here, p and F_c are determined from the load versus COD curve (ISRM 1988). We used $D = 60$ mm, $a_0 = 9$ mm, and $S = 99.9$ mm in accordance

with the suggested method (ISRM 1988) and the specimens were made with their notches in the arrester orientation with respect to the bedding planes.

2.3 Numerical Model by DEM

Analytical methods based on continuum mechanics are normally used in the design of many geological structures, such as roadway tunnels. However, it is difficult to use continuum mechanics to simulate failures like the separation of materials and shear planes. In this study, a DEM-based two-dimensional discontinuum program called PFC2D (Itasca Consulting Group Inc. 2004) is used to simulate crack propagation in rocks. PFC2D simulates the mechanical behavior of a material by representing it as an assemblage of circular particles that can be bonded to one another. The basic mechanical properties such as Young's modulus and Poisson's ratio are derived from laboratory tests. In the continuum model, the elastic properties can be used directly. However, in PFC2D, the mechanical behavior of the assemblage is dominated by the microproperties of the particles and the bonds between them. These microproperties cannot be determined from laboratory tests. Thus, the relationship between the microproperties and the macroproperties should be determined by the modeling of rock testing, such as the uniaxial compressive strength (UCS) test and the Brazilian test, prior to the simulation of fracture toughness. Moreover, a clumped particle model (Cho et al. 2007), which combines particles located within a circle, is adopted in this study; each clump behaves as an element having a complicated shape.

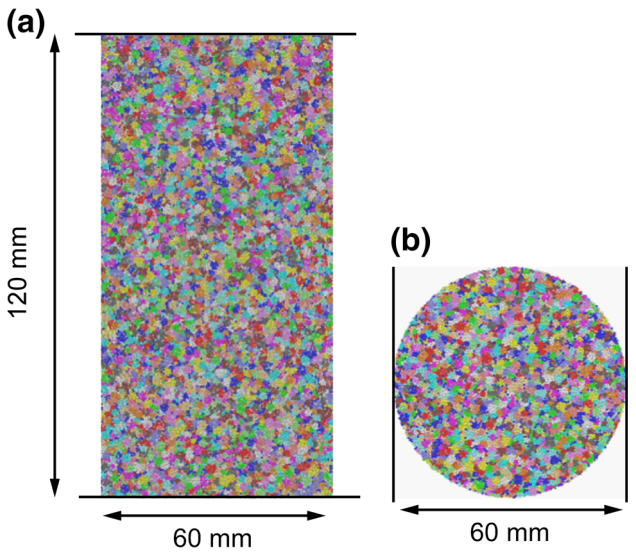

Fig. 5 Distinct element method (DEM) models of: **a** the uniaxial compressive test and **b** the Brazilian test (Funatsu et al. 2008)

2.3.1 *Numerical Modeling of the Uniaxial Compressive and Brazilian Tests*

Simulations of the uniaxial compressive and Brazilian tests were conducted to calibrate the appropriate input parameters. These simulations were performed according to the works of Potyondy and Cundall (2004). The specimen for the compressive tests is 120 mm in length and 60 mm in width, and the diameter of the specimen for the Brazilian tests is 60 mm. Both the particles and models themselves have thicknesses of one unit of length, which is equal to 1 m. The calibration process is explained in detail by Funatsu et al. (2008). The number of particle elements is about 21,000 for the uniaxial compressive test model. Being a two-dimensional code, the PFC2D is unable to simulate the compressive test of a cylindrical specimen. Therefore, we decided to simulate the compressive test of a rectangular specimen having unit thickness.

For the uniaxial compressive tests, the top and bottom wall elements act as the loading platens, and the velocity of the walls is kept constant at 5.0×10^{-5} mm/step (i.e., the rate of load application). For the Brazilian tests, the side walls act as platens, and the velocity of the walls is kept constant at 5.0×10^{-5} mm/step. The models for the uniaxial compressive tests and Brazilian tests are shown in

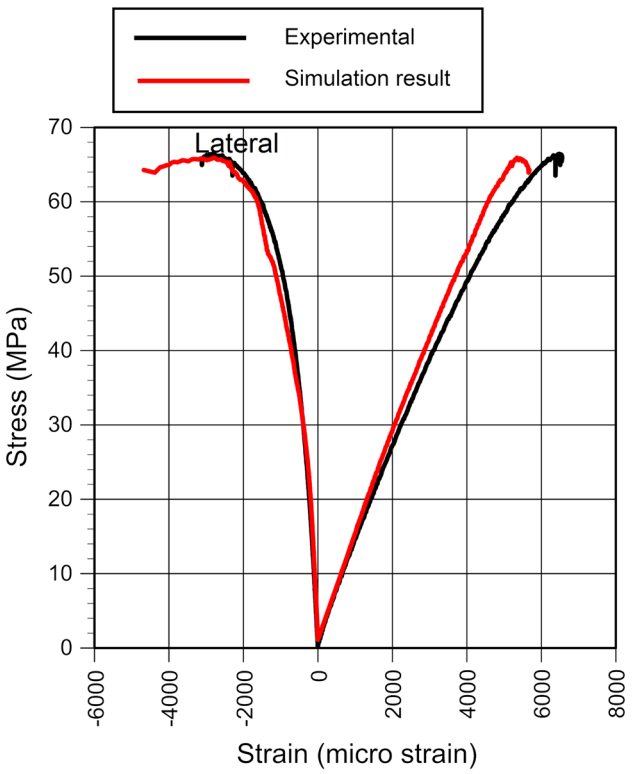

Fig. 6 Comparison of the stress–strain curves of the uniaxial compressive test; experimental and numerical simulation (Funatsu et al. 2008)

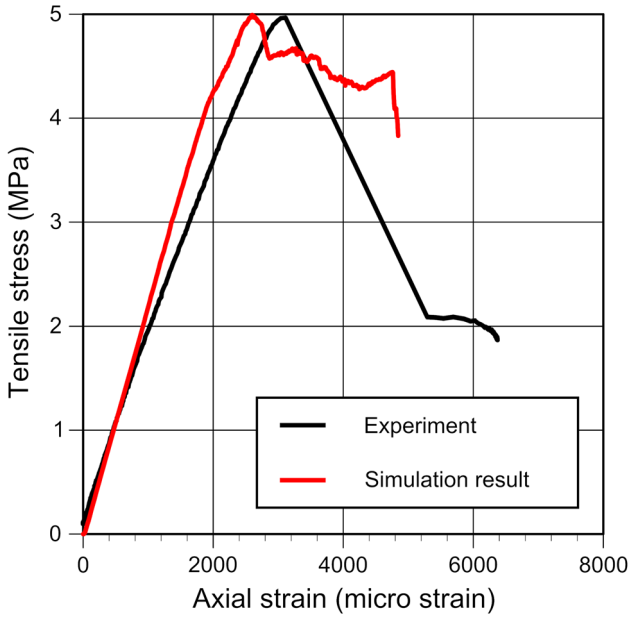

Fig. 7 Comparison of the stress–strain curves of the Brazilian test; experimental and numerical simulation (Funatsu et al. 2008)

Fig. 5. The applied stress is measured by dividing the average force acting on opposing walls by the area of the corresponding specimen cross-section (Potyondy and Cundall 2004).

Figures 6 and 7 show the stress–strain curves derived by the physical tests, along with the results of the simulating UCS and Brazilian tests, respectively. With the appropriate selection of DEM parameters, it can be seen that the model simulates the experimental results very well. This is despite the fact that a two-dimensional rectangular model was used, which is expected to be weaker in compression than if a cylindrical model was used. The crack distribution indicates that tensile failure occurs along the loading direction. The tensile strength calculated by the numerical model of the Brazilian test is 5.0 MPa. The difference in tensile strength between the numerical simulation and the experiments is only 0.1 MPa. However, there is a limitation of the numerical model in comparison with the test specimen. The former is a two-dimensional model and the latter is a three-dimensional cylindrical shape. Cho et al. (2007) showed that the two-dimensional clumped particle model can reproduce the failure envelope of both hard rock and weak rock. Our results support their findings. A set of input parameters suitable for the modeling of Kimachi sandstone is given in Table 2.

2.3.2 Modeling of the SCB Specimen by DEM

The model of the SCB specimen is shown in Fig. 8b. Figure 8a shows the SCB specimen for comparison. The notch is created by deleting the particles located within the notch. The specimen diameter is 100 mm and initial notch length is 25 mm. The thickness of the test specimen is 25 mm. The numerical model is of unit length thickness (1 m). The support and loading rollers for three-point bending are created by wall elements. The support rollers are kept separated by a fixed span length of 80 mm, which is same as that used in the physical tests. The element size was defined as shown in Table 2. The particles were randomly packed with a uniform size distribution. The number of particles was 11,663. The loading roller located above the specimen is made to move downward at a constant displacement rate of 5.0×10^{-6} mm/step. The loading force used to evaluate the fracture toughness is taken as the force acting between the loading roller and the adjacent material particles. The displacement of the loading roller and the COD is also monitored. In PFC2D, stress cannot be calculated directly; instead, it is calculated as an average value inside the representative area, namely, the measurement circle. The radius of the circle is 3.0 mm, which is three times larger than the average radius of a clump. This diameter was selected to allow estimation of the proper stress state. The measurement circle was located in front of the initial notch tip. Since the stress calculated by the measurement circle is the average value inside the circle, the stress near the notch tip can be underestimated in the case of having a measurement circle with a large radius. In addition, if the crack extends during loading, the calculated stress change can be attenuated by the effect of averaging because the minimum crack extension is 0.2 mm, which is the same value as the minimum ball radius and is smaller than the radius of the measurement circle.

A microcracking in the numerical simulation is defined as a bond breakage between particles. The crack extension is defined as the length from the crack tip to the farther end of the connecting microcracks.

Table 2 Microscopic parameters for distinct element method (DEM) modeling of Kimachi sandstone (Funatsu et al. 2008)

Parameter	Value
Minimum ball radius (mm)	0.2
Ball size ratio	1.5
Contact modulus (GPa)	2.8
Normal/shear stiffness ratio	1.5
Friction coefficient	0.2
Ball density (kg/m^3)	2,630
Parallel-bond modulus (GPa)	2.8
Parallel-bond stiffness ratio	1.5
Parallel-bond radius multiplier	1
Parallel-bond normal strength (MPa)	6 ± 0.6
Parallel-bond shear strength (MPa)	55 ± 5.5
Clump radius (mm)	1.0 ± 0.2

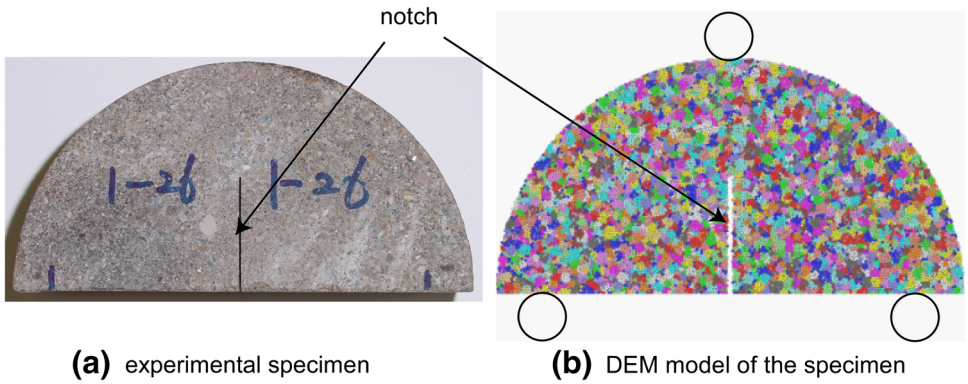

Fig. 8 SCB specimen configurations used for the (**a**) experimental and (**b**) DEM model. The specimen diameter D is 100 mm, crack length a is 25 mm, thickness t is 25 mm for the test specimen and 1 m for the DEM model, and the span length between the two bottom supports $2S$ is 80 mm

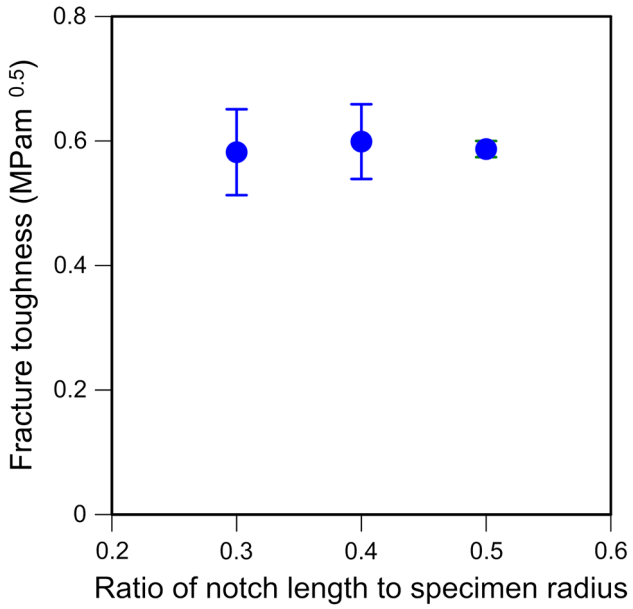

Fig. 9 Experimentally determined fracture toughness using SCB specimens

3 Results

3.1 Fracture Toughness of Kimachi Sandstone Measured Experimentally Using SCB and CB Specimens

Figure 9 shows the test results for the fracture toughness using SCB specimens. The dots and bars in the figure respectively indicate the average and standard deviation of the fracture toughness values for the same ratio of notch length to specimen radius. Three tests were performed at each crack length. This figure shows that the fracture toughness measured using SCB specimens is independent of the notch length. The average value of fracture toughness using all data is 0.589 MPam$^{0.5}$, with a standard deviation of 0.0474 MPam$^{0.5}$.

The fracture toughness measured using CB specimens is summarized in Table 3. This table shows the level I

Table 3 Summary of fracture toughness test results using chevron bend (CB) specimens

Sample ID	K_{CB} (MPam$^{0.5}$)	p	K^c_{CB} (MPam$^{0.5}$)
CB-1	0.781	0.176	0.954
CB-2	0.799	0.215	0.970
CB-3	0.798	0.271	1.053
CB-4	0.816	0.174	0.946
CB-5	0.781	0.149	0.885
Average	0.795	0.197	0.962
Standard deviation	0.0146	0.0476	0.060

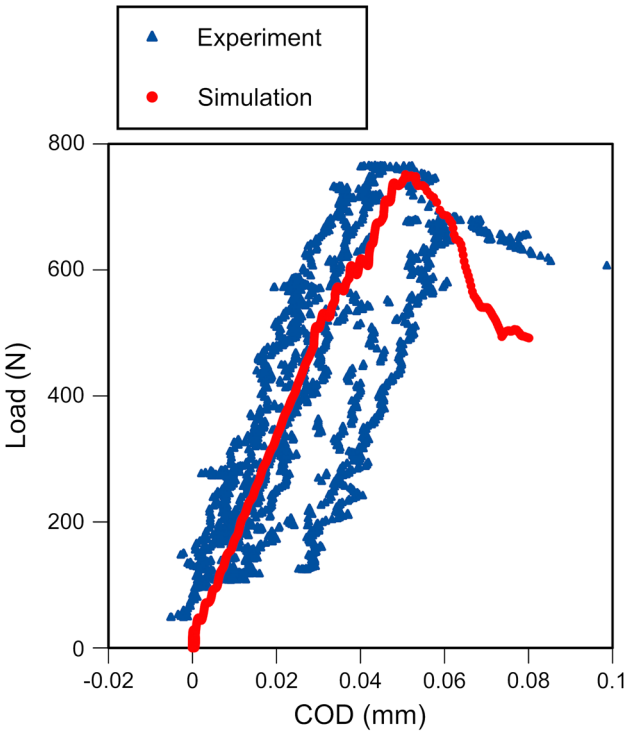

Fig. 10 Load versus COD curves obtained by numerical simulation and experimental methods. Note that the experimental graph includes partial unloading and reloading

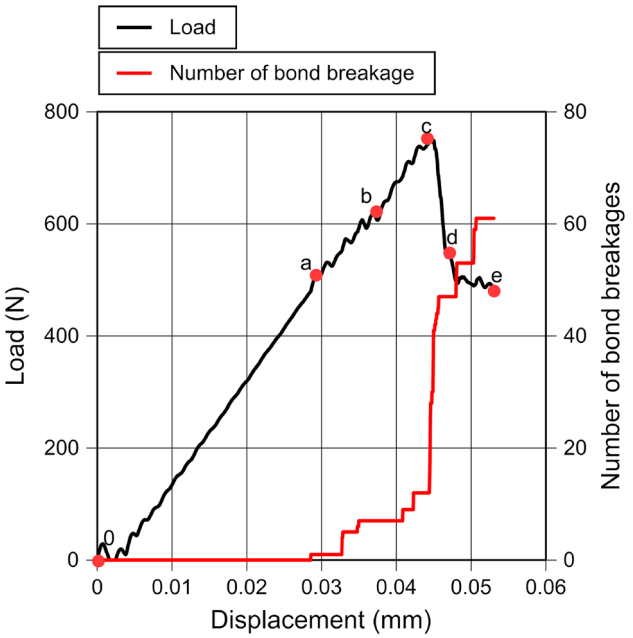

Fig. 11 Load versus displacement curve and cumulative number of bond breakages for the case of $a/R = 0.5$ obtained by numerical simulation

fracture toughness K_{CB}, the level II fracture toughness K^c_{CB}, and the degree of nonlinearity p.

The fracture toughness of Kimachi sandstone as measured using SR specimens was investigated by Matsuki et al. (1991). The level I fracture toughness K_{SR} had values of 0.86 and 0.85 MPam$^{0.5}$, with specimen diameters of 80 and 100 mm, respectively. The level II fracture toughness K^c_{SR} has values of 1.01 and 1.02 MPam$^{0.5}$, with specimen diameters of 80 and 100 mm, respectively. The fracture toughness measured using CB specimens in this study compares well with Matsuki et al.'s results. However, the level I and level II fracture toughness values measured using CB specimens are, respectively, ~35 and 63 % higher than those measured using SCB specimens.

3.2 Numerical Simulation of Fracture Toughness using the SCB Specimen

Figure 10 shows the load–COD curves determined by numerical modeling and through experimental results. The experimental result was from a typical test involving partial unloading cycles as shown in the figure. Note that, in the simulation, the specimen thickness was set to 1 m. Therefore, the load shown in the figure was converted from that corresponding to the thickness of 25 mm used in the experiment. The maximum load and the corresponding COD value were almost the same in the two sets of graphs. The fracture toughness determined by numerical modeling is 0.526 MPam$^{0.5}$, which is ~10 % lower than the average

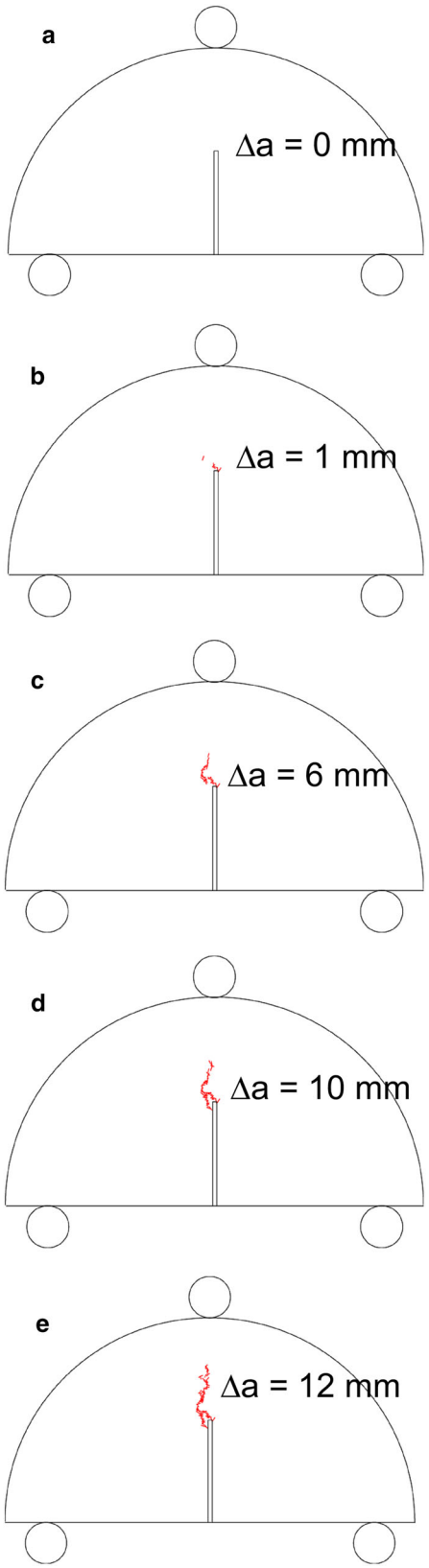

Fig. 12 Numerically determined crack growth during loading (the *dots* indicate the location of bond breakages) for a specimen with $a/R = 0.5$

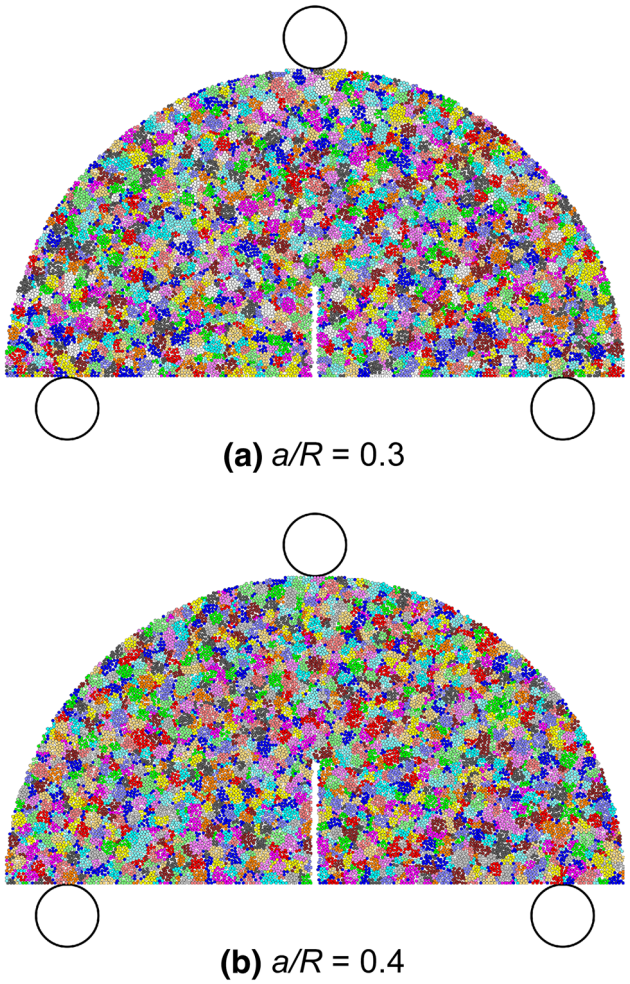

Fig. 13 SCB specimen model with (**a**) $a/R = 0.3$ and (**b**) $a/R = 0.4$

value of the fracture toughness measured experimentally using SCB specimens.

4 Discussion

4.1 Mode I Fracture Toughness Measured by SCB and CB Tests

There are only a limited number of studies comparing the fracture toughness values measured using SCB specimens and ISRM suggested methods. Chang et al. (2002) compared the fracture toughness values determined using several different types of specimens, such as SCB, CB, CCNBD, and chevron-notched SCB specimens. The fracture toughness values of granite and marble measured using SCB specimens were 0.68 and 0.871 MPam$^{0.5}$, respectively. The level I fracture toughness values of granite and marble measured using CB specimens were ~1.4 and 1.1 MPam$^{0.5}$, respectively. These values are

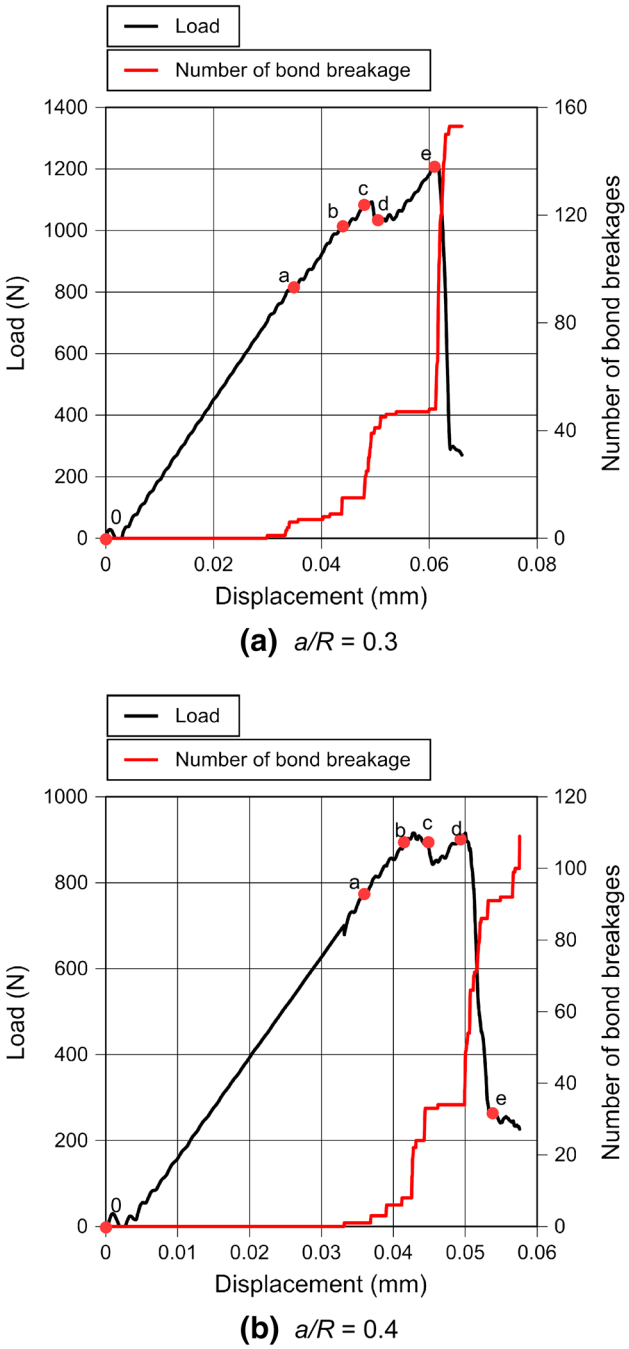

Fig. 14 Load versus displacement curves and cumulative number of bond breakages obtained by numerical simulation: **a** $a/R = 0.3$ and **b** $a/R = 0.4$

almost the same as those measured using CCNBD specimens. Tutluoglu and Keles (2011) reported that the level I fracture toughness values of andesite measured using SCB and CCNBD specimens were 0.94 and 1.45 MPam$^{0.5}$, respectively. Our results using sandstone showed that the trend is the same, i.e., the fracture toughness measured using SCB specimens is lower than that measured using CB and CCNBD specimens. One of the reasons for the

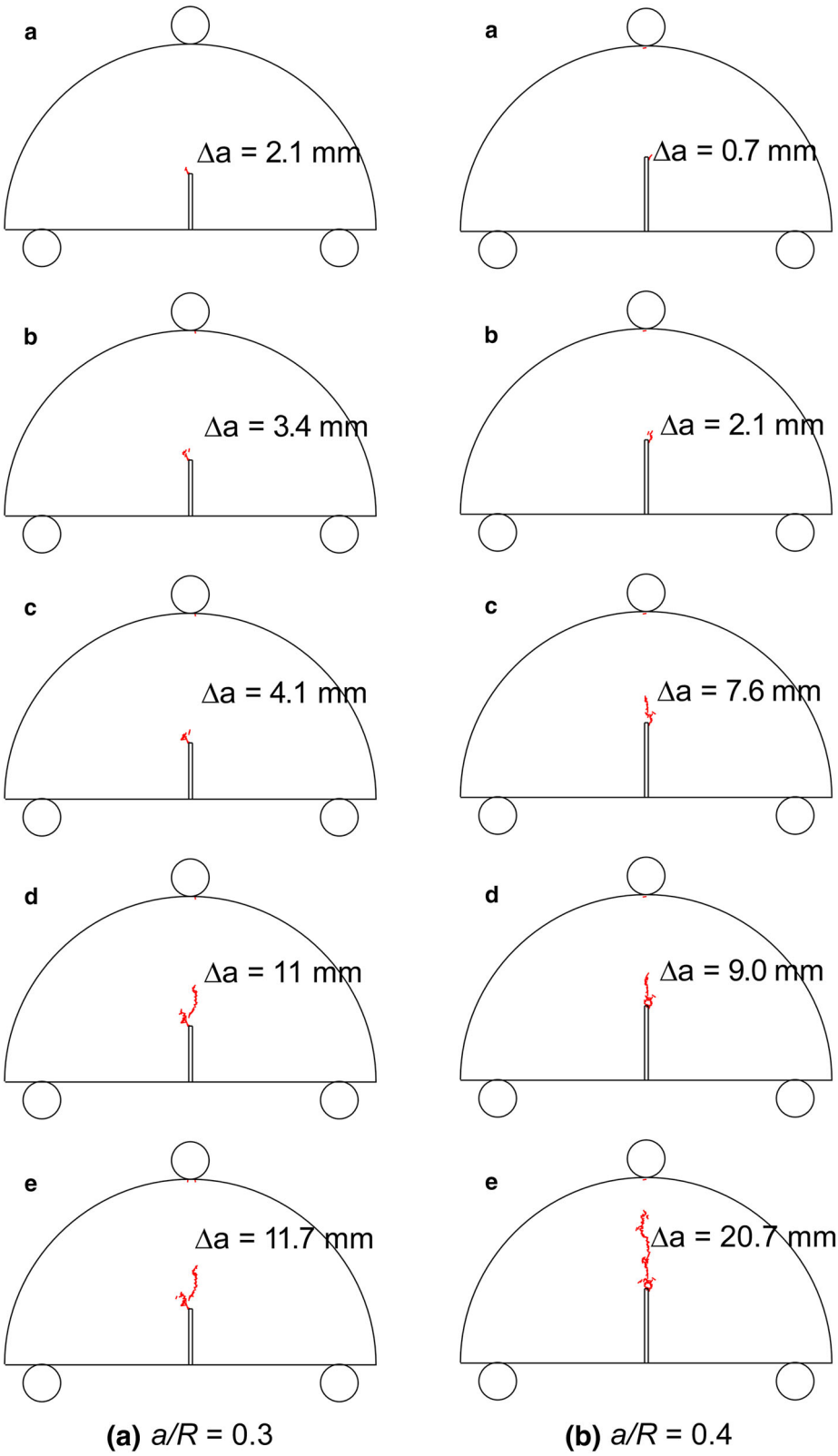

Fig. 15 Numerically determined crack growth during loading (the *dots* indicate the location of bond breakages) for a specimen with **a** $a/R = 0.3$ and **b** $a/R = 0.4$

Table 4 Values used in the development of the stress intensity factor for (a) $a/R = 0.3$, (b) $a/R = 0.4$, and (c) $a/R = 0.5$

Part	R (mm)	S (mm)	t (mm)	a_0 (mm)	Δa (mm)	a (mm)	a/R (–)	F (N)	σ_0 (MPa)	Y (–)	K_{SCB} (MPam$^{0.5}$)
(a) $a/R = 0.3$											
0	50	40	25	15	0	15	0.3	0	0	4.36	0
a	50	40	25	15	2.1	17.1	0.34	806.3	0.323	4.55	0.34
b	50	40	25	15	3.4	18.4	0.37	1011.6	0.405	4.72	0.46
c	50	40	25	15	4.1	19.1	0.38	1077.8	0.431	4.84	0.51
d	50	40	25	15	11.0	26.0	0.52	1036.9	0.415	6.59	0.78
e	50	40	25	15	11.7	26.7	0.53	1211.4	0.485	6.84	0.96
(b) $a/R = 0.4$											
0	50	40	25	20	0	20	0.4	0	0	5.00	0
a	50	40	25	20	0.7	21	0.41	793.7	0.317	5.14	0.42
b	50	40	25	20	2.1	22	0.44	906.5	0.363	5.45	0.52
c	50	40	25	20	7.6	28	0.55	906.5	0.363	7.19	0.77
d	50	40	25	20	9.0	29	0.58	911.9	0.365	7.79	0.86
e	50	40	25	20	20.7	41	0.81	286.1	0.114	23.52	0.96
(c) $a/R = 0.5$											
0	50	40	25	25	0	25	0.5	0	0	6.26	0
a	50	40	25	25	0.0	25.0	0.5	474.2	0.190	6.26	0.33
b	50	40	25	25	1.0	26.0	0.52	616.7	0.247	6.59	0.46
c	50	40	25	25	6.0	31.0	0.62	744.1	0.298	8.91	0.83
d	50	40	25	25	10.0	35.0	0.7	548.5	0.219	12.38	0.90
e	50	40	25	25	12.0	37.0	0.74	480.0	0.192	15.18	1.00

difference in fracture toughness is the different notch type. Both the CB and CCNBD specimens have a chevron notch, whereas the SCB specimen has a straight notch. Furthermore, differences may exist in the development of the process zone, as it is affected by the type of loading, e.g., bending versus tension. Khan and Al-Shayea (2000) found that the fracture toughness values of limestone measured using CSTBD and CCNBD specimens were, respectively, 0.42 and 0.61 MPam$^{0.5}$. Chang et al. (2002) reported that the fracture toughness values measured using chevron-notched SCB specimens for granite and marble were 1.39 and 1.11 MPam$^{0.5}$, respectively. These values are $\sim$2 times and 1.2 times higher than those measured using straight notched SCB specimens. In order to satisfy the requirements of LEFM on which the fracture toughness is based, the size of the FPZ during loading should be small enough so that the material behavior of the rock sample can be considered as linearly elastic. The radius of the FPZ can be derived from the following equation (Schmidt 1980):

$$r_c = \frac{1}{2\pi}\left(\frac{K_{Ic}}{\sigma_t}\right)^2 \tag{6}$$

For Kimachi sandstone, the value of r_c calculated using the level II fracture toughness measured using CB specimens is 6.13 mm. The actual notch length and other dimensions need to be much larger than r_c. Furthermore, the fracture toughness may be underestimated unless (1) the crack starts to propagate when the FPZ is fully developed and (2) the fracture toughness is evaluated when the slow stable crack growth reaches its critical limit. The large difference in fracture toughness measured for CB and SCB specimens shows that the level I fracture toughness of the SCB specimen fails to satisfy those conditions.

4.2 Evaluation of Fracture Toughness by the *K*-Resistance Curve

When evaluating the fracture toughness, the crack growth that occurs at the critical level of loading cannot be ignored. If the crack growth is measured, the fracture toughness can be corrected as a function of the actual crack length using the *K*-resistance curve. In this study, we evaluated the crack growth by numerical modeling based on DEM. Figure 11 shows the load versus load-line displacement curve, as obtained by numerical modeling. The number of bond breakages corresponding to microcracking is also shown. The bond breakages suggest that a crack initiates before the load reaches the maximum value and that it propagates rapidly when the load reaches the maximum.

Figure 12 shows the crack growth during loading based on the numerical simulation. The crack growth at each

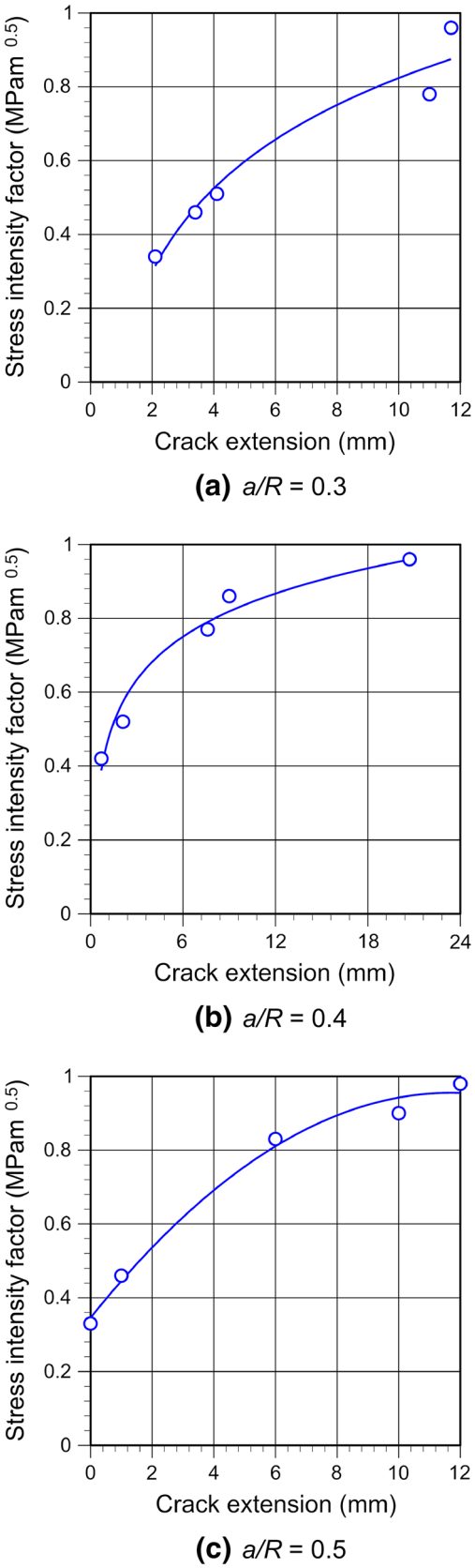

Fig. 16 *K*-resistance curves for Kimachi sandstone for: **a** $a/R = 0.3$, **b** $a/R = 0.4$, and **c** $a/R = 0.5$

point and the corresponding load can be derived from the numerical modeling. Parts a, b, c, d, and e in Fig. 12 correspond to points a, b, c, d, and e in Fig. 11. The crack growth at the maximum load is ~6 mm, as given in Fig. 12c. Furthermore, Fig. 12d shows the occurrence of sudden, unstable crack growth when the maximum load is reached. Following Eq. (1), the mode I stress intensity factor K_I at each point can be calculated as:

$$K_I = YF\sqrt{\pi(a + \Delta a)}\Big/2Rt \tag{7}$$

where F is the load at each evaluation point and Δa is the crack extension at that point. Y is the normalized stress intensity factor that corresponds to the notch length $a + \Delta a$. Similarly, we conducted a numerical simulation of the crack growth of specimens having $a/R = 0.3$ and 0.4, and constructed the *K*-resistance curves. Figure 13 shows the DEM models of an SCB specimen having $a/R = 0.3$ and $a/R = 0.4$, respectively.

Figure 14 shows the load and the number of bond breakages versus the load-line displacement, and Fig. 15 shows the crack growths for those two cases. Table 4 gives a summary of the values of important parameters in the development of the stress intensity factor for $a/R = 0.3$, $a/R = 0.4$, and $a/R = 0.5$, respectively, and Fig. 16 shows the development of the stress intensity factor with crack growth, which is the *K*-resistance curve. These figures show that the fracture toughness is about 0.95 $MPam^{0.5}$, which is comparable to the level II fracture toughness obtained for the CB specimen.

The fundamental process of macrocrack extension in brittle rock is almost always by the opening, growth, and coalescence of microcracks that occurs within the process zone. Barker's nonlinearity correction incorporates the effect of the finite size of the process zone and yields an improved value known as the level II fracture toughness (Barker 1977). On the other hand, the *K*-resistance curve indirectly measures the energy release rate with the development of the process zone and, therefore, the two methods are expected to result in the same value for fracture toughness.

5 Conclusions

To investigate the mode I fracture toughness using semi-circular bend (SCB) specimens, we experimentally studied the fracture toughness using SCB and chevron bend (CB) specimens, the latter being one of the International Society for Rock Mechanics (ISRM) suggested methods, for comparison. The mode I fracture toughness measured using SCB specimens is lower than the level I and level II fracture toughness values measured using CB specimens.

This difference is attributed to differences in notch type, neglecting the stable crack extension, and the differences in the fracture process zone (FPZ) sizes.

A numerical study based on discontinuum mechanics was conducted to evaluate crack propagation in the SCB specimen during loading. The numerical result is validated by comparing the load versus crack-opening displacement (COD) curves obtained by the numerical model and by the experiments. The results show that subcritical crack growth, as well as sudden crack propagation, occurs when the load reaches the maximum. For the specimen sizes used for the tests, the crack extension at the maximum load is less than ~ 7 mm. This is almost the same as the radius of the FPZ as calculated by Schmidt's formula.

Moreover, the *K*-resistance curve is determined using the crack extension and the stress intensity factor at the evaluation point. The resistance increases with crack growth and reaches a steady value, which is considered to be the fracture toughness. The fracture toughness evaluated in this matter is in agreement with the level II fracture toughness measured using CB specimens. Therefore, the results show that an improved value for fracture toughness can be determined when the resistance to crack propagation is considered. The suggested numerical method enables the fracture toughness (which is comparable to that given by the ISRM suggested CB specimen method) to be determined by measuring the *K*-resistance during stable crack propagation in SCB specimens.

Acknowledgments We would like to thank Ms. Qian Li for her help with running the simulations.

References

Aliha MRM, Sistaninia M, Smith DJ, Pavier MJ, Ayatollahi (2012) Geometry effects and statistical analysis of mode I fracture in guiting limestone. Int J Rock Mech Min Sci 51:128–135. doi:10.1016/j.ijrmms.2012.01.017

Azevedo NM, Lemos JV (2006) Hybrid discrete element/finite element method for fracture analysis. Comput Methods Appl Mech Eng 195(33–36):4579–4593. doi:10.1016/j.cma.2005.10.005

Barker LM (1977) A simplified method for measuring plane strain fracture toughness. Eng Fract Mech 9:361–369

Chang SH, Lee CI, Jeon S (2002) Measurement of rock fracture toughness under modes I and II and mixed-mode conditions by using disc-type specimens. Eng Geol 66(1–2):79–97. doi:10.1016/s0013-7952(02)00033-9

Cho N, Martin CD, Sego DC (2007) A clumped particle model for rock. Int J Rock Mech Min Sci 44(7):997–1010. doi:10.1016/j.ijrmms.2007.02.002

Chong KP, Kuruppu MD (1988) New specimens for mixed mode fracture investigations of geomaterials. Eng Fract Mech 30(5):701–712. doi:10.1016/0013-7944(88)90160-9

Chong KP, Kuruppu MD, Kuszmaul JS (1987) Fracture toughness determination of layered materials. Eng Fract Mech 28(1):43–54

Cundall PA, Strack OD (1979) A discrete numerical model for granular assemblies. Geotech 29(1):47–65

D'Addetta GA, Kun F, Ramm E (2002) On the application of a discrete model to the fracture process of cohesive granular materials. Granul Matter 4(2):77–90. doi:10.1007/s10035-002-0103-9

Dai F, Xia K, Nasseri MHB, Mohanty B (2007) Crack microcrack interaction and fracture toughness anisotropy in rocks. In: Proceedings of the SEM annual conference and exposition on experimental and applied mechanics, Springfield, MA, USA, June 2007, pp 1383–1390

Fowell RJ (1995) Suggested method for determining mode I fracture toughness using cracked chevron notched Brazilian disc (CCNBD) specimens. Int J Rock Mech Min Sci Geomech Abstr 32(1):57–64. doi:10.1016/0148-9062(94)00015-U

Fowell RJ, Xu C (1994) The use of the cracked Brazilian disc geometry for rock fracture investigations. Int J Rock Mech Min Sci Geomech Abstr 31(6):571–579

Funatsu T, Seto M, Shimada H, Matsui K, Kuruppu M (2004) Combined effects of increasing temperature and confining pressure on the fracture toughness of clay bearing rocks. Int J Rock Mech Min Sci 41(6):927–938. doi:10.1016/j.ijrmms.2004.02.008

Funatsu T, Li Q, Shimizu N, Seto M, Matsui K (2008) Numerical simulation of crack propagation in rock by particle flow code. J MMIJ 124(10–11):611–618

Guo H, Aziz NI, Schmidt LC (1993) Rock fracture-toughness determination by the Brazilian test. Eng Geol 33(3):177–188. doi:10.1016/0013-7952(93)90056-I

International Society for Rock Mechanics (ISRM) (1988) Suggested methods for determining the fracture toughness of rock. Int J Rock Mech Min Sci Geomech Abstr 25(2):71–96. doi:10.1016/0148-9062(88)91871-2

Iqbal MJ, Mohanty B (2007) Experimental calibration of ISRM suggested fracture toughness measurement techniques in selected brittle rocks. Rock Mech Rock Eng 40(5):453–475. doi:10.1007/s00603-006-0107-6

Itasca Consulting Group Inc. (2004) Particle flow code in 2-dimensions (PFC2D) version 3.10, Minneapolis, MN

Khan K, Al-Shayea NA (2000) Effect of specimen geometry and testing method on mixed mode I–II fracture toughness of a limestone rock from Saudi Arabia. Rock Mech Rock Eng 33(3):179–206. doi:10.1007/s006030070006

Kuruppu MD, Obara Y, Ayatollahi MR, Chong KP, Funatsu T (2014) ISRM-suggested method for determining the mode I static fracture toughness using semi-circular bend specimen. Rock Mech Rock Eng 47(1):267–274. doi:10.1007/s00603-013-0422-7

Lim IL, Johnston IW, Choi SK, Boland JN (1994) Fracture testing of a soft rock with semi-circular specimens under three-point bending. Part 1—mode I. Int J Rock Mech Min Sci Geomech Abstr 31(3):185–197. doi:10.1016/0148-9062(94)90463-4

Matsuki K, Hasibuan SS, Takahashi H (1991) Specimen size requirements for determining the inherent fracture toughness of rocks according to the ISRM suggested methods. Int J Rock Mech Min Sci Geomech Abstr 28(5):365–374. doi:10.1016/0148-9062(91)90075-W

Nasseri MHB, Mohanty B, Young RP (2006) Fracture toughness measurements and acoustic emission activity in brittle rocks. Pure Appl Geophys 163(5–6):917–945. doi:10.1007/s00024-006-0064-8

Ouchterlony F (1981) Extension of the compliance and stress intensity formulas for the single edge crack round bar in bending. ASTM STP 745:237–256

Potyondy DO, Cundall PA (2004) A bonded-particle model for rock. Int J Rock Mech Min Sci 41(8):1329–1364. doi:10.1016/j.ijrmms.2004.09.011

Schmidt RA (1980) A microcrack model and its significance to hydraulic fracturing and fracture toughness testing. In: Proceedings of the 21st U.S. symposium on rock mechanics (USRMS), Rolla, MO, USA, May 1980, pp 581–590

Tan Y, Yang D, Sheng Y (2009) Discrete element method (DEM) modeling of fracture and damage in the machining process of polycrystalline SiC. J Eur Ceram Soc 29(6):1029–1037. doi:10.1016/j.jeurceramsoc.2008.07.060

Tutluoglu L, Keles C (2011) Mode I fracture toughness determination with straight notched disk bending method. Int J Rock Mech Min Sci 48(8):1248–1261. doi:10.1016/j.ijrmms.2011.09.019

Wang Q-Z, Xing L (1999) Determination of fracture toughness K_{IC} by using the flattened Brazilian disk specimen for rocks. Eng Fract Mech 64:193–201